

Influence of friction on the packing efficiency and short-to-intermediate range structure of hard-sphere systems

Cite as: J. Chem. Phys. 159, 194901 (2023); doi: 10.1063/5.0175513

Submitted: 7 September 2023 • Accepted: 25 October 2023 •

Published Online: 15 November 2023



Jiajun Tang,¹ Xiaohui Wen,¹ Zhen Zhang,^{1,a)} Deyin Wang,^{1,2} Xinbiao Huang,¹ and Yujie Wang^{1,3,4,a)}

AFFILIATIONS

¹ College of Mathematics and Physics, Chengdu University of Technology, Chengdu 610059, China

² School of Physics, Zhejiang University, Hangzhou 310027, China

³ State Key Laboratory of Geohazard Prevention and Geoenvironment Protection, Chengdu University of Technology, Chengdu 610059, China

⁴ School of Physics and Astronomy, Shanghai Jiao Tong University, Shanghai 200240, China

^{a)} Authors to whom correspondence should be addressed: zhen.zhang@cdut.edu.cn and yujiewang@sjtu.edu.cn

ABSTRACT

Using particle-resolved computer simulations, we investigate the effect of friction on the packing structure of hard-sphere mixtures with two kinds of particles under external compression. We first show that increasing friction between the particles results in a more disordered and less efficient packing of the local structure on the nearest neighbor scale. It is also found that standard two-point correlation functions, i.e., radial distribution function and static structure factor, show basically no detectable changes beyond short-range distances upon varying inter-particle friction. Further analysis of the structure using a four-point correlation method reveals that these systems have on the intermediate-range scale a three-dimensional structure with an icosahedral/dodecahedral symmetry that exhibits a pronounced dependence on friction: small friction gives rise to an orientational order that extends to larger distances. Our results also demonstrate that composition plays a role in that the degree of structural order and the structural correlation length are mainly affected by the friction coefficients associated with the more abundant species.

Published under an exclusive license by AIP Publishing. <https://doi.org/10.1063/5.0175513>

I. INTRODUCTION

Hard-sphere systems are useful models to explore the diverse behaviors of various disordered systems, such as simple liquids, colloids, and metallic glasses. Characterizing the structure of hard-sphere systems has proven to be a crucial step toward understanding the physical properties of disordered systems.^{1–7} In particular, particle-resolved experiments and computer simulations have shown that the local structure of hard-sphere-like systems, such as colloidal liquids, is surprisingly varied.^{8–11} The type and concentration of these local structures are functions of multiple factors, such as packing fraction, composition, particle size disparity, and interaction energy between particles.^{12–19} However, beyond the local level, knowledge about the structure on larger length scales is very limited.^{20–26}

Using numerical simulations, Tanaka and co-workers have discovered the presence of medium-range order in hard-sphere liquids,

characterized by the formation of clusters with pronounced crystalline order,^{22,25,26} these initially isolated clusters grow (up to a size of around ten particle diameters) and survive for a longer time upon supercooling, which has been linked to the slow glassy dynamics on approaching the glass transition.²² Aside from these arguments on the presence of crystalline medium-range order, standard structural quantities, such as the static structure factor, are also instructive to learn the change of intermediate-range structural order. However, these standard structural quantities give no insights into the three-dimensional (3D) (i.e., orientation-dependent) structure of a 3D system, thus hindering our understanding of the macroscopic properties of disordered systems from a structural perspective. In a recent study, Zhang and Kob proposed a four-point correlation method that is capable of measuring the 3D structure of particle-resolved disordered systems beyond short-range distances.²⁷ Application of this method to experimental granular and colloid systems has revealed the presence of icosahedral/dodecahedral orientational

order extending to intermediate and large distances. Moreover, it has been shown that these intermediate-range structures are strongly connected to macroscopic properties, such as particle packing efficiency and liquid dynamics.^{28,29}

When friction is present, the packing structure of the particles can be altered from random close packing to random loose packing,^{1,30–35} which has a direct impact on the mechanical stability of the structure.^{36–39} Previous studies have mainly focused on the effect of friction on the local packing structure of hard-sphere systems, while the structural information on larger length scales was scarce, probably because standard structural measures do not seem to reveal interesting structures beyond, say the first two nearest neighbor shells.

In this work, we are motivated to understand the effect of inter-particle friction on the structure of hard-sphere systems comprised of two kinds of particles, with a particular focus on revealing the hidden structural order beyond nearest neighbor distances. We first analyze the effect of friction on the local structure in terms of the particle's Voronoi volume and local orientational order parameter. Then, we present the standard two-point structural quantities, such as the radial distribution function and static structure factor, and demonstrate that they are not sensitive to the change of particle friction. Further analysis of the structure using a more advanced four-point correlation method allows revealing the presence of a 3D orientational order on the intermediate length scale and exhibits a strong dependence on the change of friction between particles.

The rest of this paper is organized as follows: Sec. II describes the details of the model and simulation method used in this study. In Sec. III, we present and discuss the main results. Finally, we summarize the findings of this work in Sec. IV.

II. MODEL AND SIMULATION METHOD

Molecular dynamics simulations of particles with static friction were performed using the Large-scale Atomic/Molecular Massively Parallel Simulator (LAMMPS) software.⁴⁰ We studied a binary mixture of particles (of types A and B) having the same diameter but different coefficients of friction. Interactions between the particles were given by the Hertz-Mindlin no-slip model,⁴¹ which has been successfully applied in previous studies to probe the properties of particle systems.^{42–44} The normal component $F_{ij}^{(n)}$ and tangential

component $F_{ij}^{(t)}$ of the contact force between particles i and j are expressed as

$$\mathbf{F}_{ij}^{(n)} = \frac{4}{3} E_{ij} (R_{ij})^{1/2} \alpha^{3/2} \mathbf{n}_{ij} - \beta_n \mathbf{v}_{ij}^{(n)}, \quad (1)$$

$$\mathbf{F}_{ij}^{(t)} = -k_t a \delta \mathbf{t}_{ij} - \beta_t \mathbf{v}_{ij}^{(t)}. \quad (2)$$

For the normal force $\mathbf{F}_{ij}^{(n)}$, $E_{ij} = [(1 - v_i^2)E_i^{-1} + (1 - v_j^2)E_j^{-1}]^{-1}$ is the effective Young's modulus, with v_i and E_i , respectively, being the Poisson ratio and Young's modulus of particle i ; $R_{ij} = (R_i^{-1} + R_j^{-1})^{-1}$ is the effective radius, with R_i being the radius of particle i ; $\alpha = R_i + R_j - \|\mathbf{r}_{ij}\|$ is the particle's normal overlap, where $\mathbf{r}_{ij} = \mathbf{r}_i - \mathbf{r}_j$ and \mathbf{r}_i is the position vector of particle i . We denote $\mathbf{n}_{ij} = \mathbf{r}_{ij}/\|\mathbf{r}_{ij}\|$ as the normal unit vector, β_n as the normal damping, and $\mathbf{v}_{ij}^{(n)} = [(\mathbf{v}_j - \mathbf{v}_i) \cdot \mathbf{n}_{ij}] \mathbf{n}_{ij}$ as the normal component of relative velocity with \mathbf{v}_i being the velocity vector of particle i . For the tangential force $\mathbf{F}_{ij}^{(t)}$, $k_t = 8G_{ij}$, where $G_{ij} = [(1 - v_i^2)G_i^{-1} + (1 - v_j^2)G_j^{-1}]^{-1}$ is the effective shear modulus with G_i being the shear modulus of particle i ; $a = \sqrt{R_{ij}}\alpha$ is the radius of the contact region, which is perpendicular to the line connecting the centers of the two particles when they are in contact (overlap); δ is the integrated tangential displacement, which accounts for sliding and rolling motion; β_t is tangential damping, $\mathbf{v}_{ij}^{(t)} = \mathbf{v}_j - \mathbf{v}_i - \mathbf{v}_{ij}^{(n)} - (R_i \boldsymbol{\omega}_i + R_j \boldsymbol{\omega}_j) \times \mathbf{n}$ is the relative tangential velocity at the point of contact with $\boldsymbol{\omega}_i$ being the angular velocity vector of particle i ; and $\mathbf{t}_{ij} = \mathbf{v}_{ij}^{(t)}/\|\mathbf{v}_{ij}^{(t)}\|$ is the tangential unit vector. Static friction is implemented by truncating the tangential force $\mathbf{F}_{ij}^{(t)}$ to satisfy the coulomb yield criteria $\|\mathbf{F}_{ij}^{(t)}\| < \|\mu \mathbf{F}_{ij}^{(n)}\|$, where μ is the static friction coefficient.

We used μ_{AA} to denote the friction coefficient among type A particles, μ_{BB} that of type B particles, and μ_{AB} that between type A and type B particles. All parameters were expressed in LJ reduced units, which set the four fundamental parameters of mass m , length σ , energy ϵ , and the Boltzmann constant k_B to 1. The units of other parameters were derived from these four. In our work, the parameters for different particles are the same except for friction. We used a large stiffness to make sure that the collision time between the particles is very short and the overlap is very small, giving the particles hard-sphere-like properties.

We simulated a system containing 30 000 particles. The initial simulation box has dimensions of $140 \times 140 \times 50$ ($x \times y \times z$), in

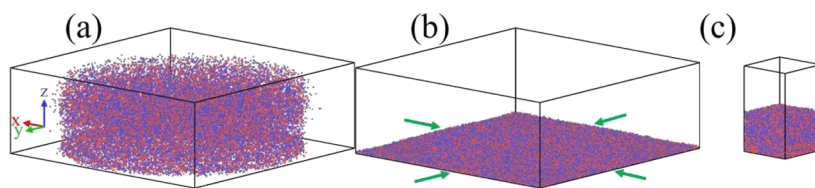


FIG. 1. Schematic illustration of the simulation process. A and B particles are colored in red and blue, respectively. The composition shown is A₅₀B₅₀. (a) Randomizing the particles in a cylinder. (b) The two-dimensional packing structure formed by the particles falling onto the bottom of the simulation box. (c) The final structure after biaxial compression.

unit of d , i.e., the diameter of the particles. We conducted simulations for 400 000 steps, with a timestep of 0.001τ (where $\tau = \sigma\sqrt{m/\epsilon}$ is the time unit), under a microcanonical ensemble. Initially, particles were randomly placed into a cylinder (with a diameter of $50d$ and a height of $140d$) and fell onto the bottom of the simulation box due to gravity, as shown in Fig. 1(a) (note that special attention was given to preclude overlapping of the particles). The particles that lay on the bottom of the box formed a loose one-layer packing structure, as depicted in Fig. 1(b). Subsequently, the box was compressed along the two axial directions parallel to the plane of the particles (note that while reducing the box's x and y dimensions, the box dimension in the z direction was kept constant). The compression rate was $0.004\tau^{-1}$, which is sufficiently small to make sure that the final structure does not depend on this rate in a significant manner (see Figs. S1–S5). The compression was terminated when the x and y dimensions were reduced to $30d$. Figure 1(c) shows a representative final structure after compression. We took the system with $\mu_{AA} = 0.1$, $\mu_{BB} = 0.2$, and $\mu_{AB} = 0.3$ as a reference for studying the influence of the three friction coefficients on the packing structure. We considered two compositions, i.e., $A_{50}B_{50}$ and $A_{80}B_{20}$, for obtaining insights into the compositional effect.

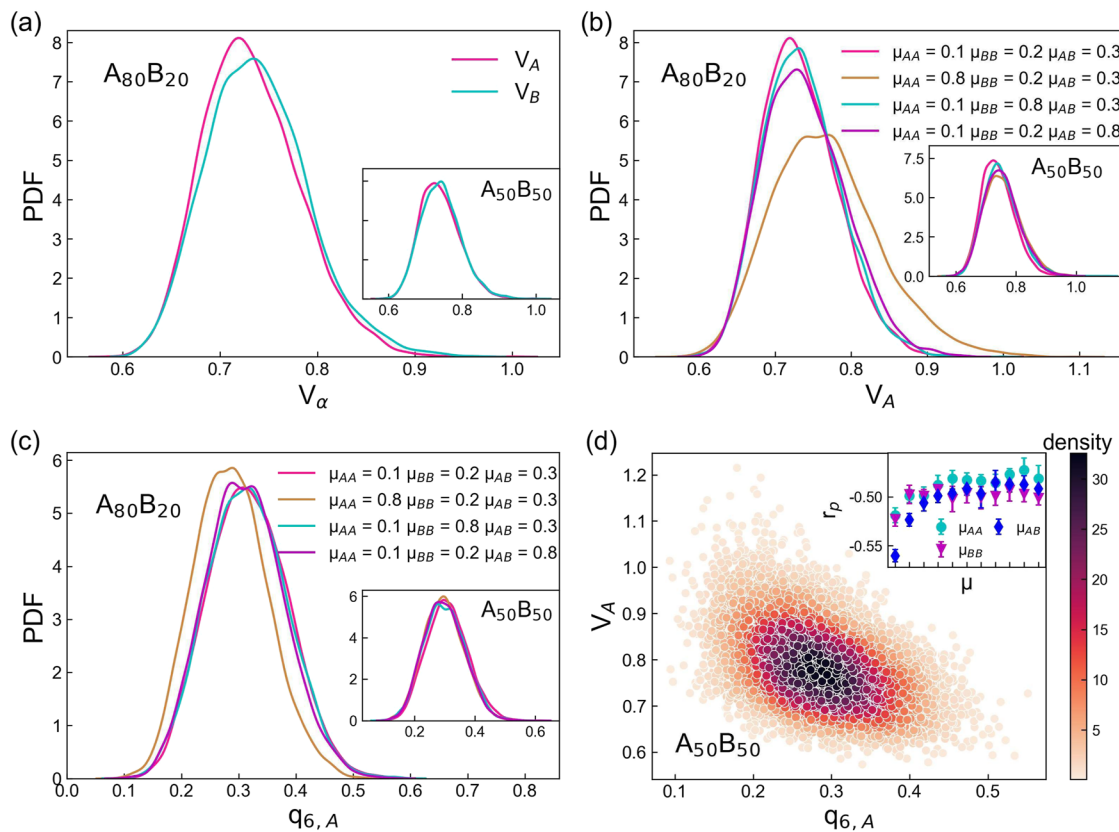


FIG. 2. Probability density function (PDF) of Voronoi volume and bond-orientational order parameter. (a) PDF of the Voronoi volume. V_α represents the Voronoi volume of type α particles. (b) PDF of V_A . (c) PDF of the bond-orientational order parameter $q_{6,A}$ of type A particles. (d) V_A vs $q_{6,A}$. The composition shown is $A_{50}B_{50}$ (with $\mu_{AA} = 0.1$, $\mu_{BB} = 0.2$, $\mu_{AB} = 0.3$). The color depends on the particle number density. Inset: The correlation coefficient r_p as functions of the friction coefficients.

III. RESULTS AND DISCUSSION

First, we show the distribution of Voronoi volume V_α and bond-orientational order parameter $q_{6,\alpha}$ as measures of local structural information of the particle type α .⁴⁵ Figure 2(a) shows that the distribution of V_α is similar between the A and B particles. Therefore, in the following, we will focus on discussing the properties of the more abundant A particles. Figure 2(b) presents the influence of friction on V_A distribution. One recognizes that μ_{AA} has the strongest effect among others, in which the distribution profile is significantly broader and shifts to larger values when μ_{AA} is increased from 0.1 to 0.8. To further quantify the local structural order of the particles, we present in Fig. 2(c) the distribution of $q_{6,A}$, which was calculated using the following expression:^{45,46}

$$q_l = \sqrt{\frac{4\pi}{2l+1} \sum_{m=-l}^{l+1} |q_{lm}^2|}, \quad (3)$$

where q_{lm} is given by

$$q_{lm} = \frac{1}{N(i)} \sum_{j=1}^{N(i)} Y_{lm}(\hat{r}_{ij}), \quad (4)$$

where i is the index of an A particle, $N(i)$ is the number of nearest neighbors of particle i , and \hat{r}_{ij} is the unit vector from particle i to particle j .

To determine the local environment of the particles, we calculated the normalized scalar product of q_{lm} ($l = 6$) using the following expression:⁴⁷

$$s(i,j) = \frac{\sum_{m=-l}^l q_{lm}(i)q_{lm}^*(j)}{\sqrt{\sum_{m=-l}^l |q_{lm}(i)|^2} \sqrt{\sum_{m=-l}^l |q_{lm}(j)|^2}}, \quad (5)$$

where j is one of the nearest neighbors of particle i and $*$ denotes complex conjugate. When the value $s(i,j)$ is larger than 0.7, the bond between i and j was considered as crystalline and otherwise disordered. If the crystalline bond of an atom exceeds 10, it is treated as crystalline.^{47,48} Based on this criterion and the broad distribution of $q_{6,A}$ [Fig. 2(c)], we confirmed that our configurations do not contain particles that can be classified as crystalline [we note that a broad yet strongly asymmetric distribution is found for the W_6 bond-orientational order invariant,⁴⁵ which is basically independent of changing the inter-particle friction (see Fig. S6)]. Figure 2(d) shows the correlation between V_A and $q_{6,A}$. Overall, one observes that larger V_A is associated with smaller $q_{6,A}$, corresponding to a more disordered structure. However, this correlation is not very strong as

seen from the Pearson correlation coefficient (r_p), depicted in the inset; V_A and $q_{6,A}$ are anti-correlated with an intermediate correlation coefficient (with an absolute value of about 0.5) that shows a slight decreasing trend as friction increases.

Further insights into the change of local structural order can be obtained by analyzing the mean and standard deviation of various quantities, as shown in Fig. 3. The increase in the mean value of V_A suggests that the particles are transitioning toward a loosely packed structure, while the increase in its standard deviation indicates that the local arrangement of particles becomes more diverse. Altogether, these results indicate that the local structure becomes more disordered with increasing particle friction. $q_{6,A}$ exhibits an opposite variation trend as seen from V_A , indicating that these two quantities are anti-correlated. The composition effect is reflected, in which as the concentration of A particles increases, the impact of the corresponding friction coefficients also becomes more pronounced. Finally, we note that, although these results consistently indicate that the local structure becomes more disordered with increasing friction coefficient, no insights on larger length scales can be obtained.

A further useful method for identifying local structures in amorphous systems is Voronoi polyhedra. We find that a large variety of polyhedral local environments coexist in the investigated systems. By counting the number of three-, four-, five-, and six-edged faces, we can construct a Voronoi index. The amount of

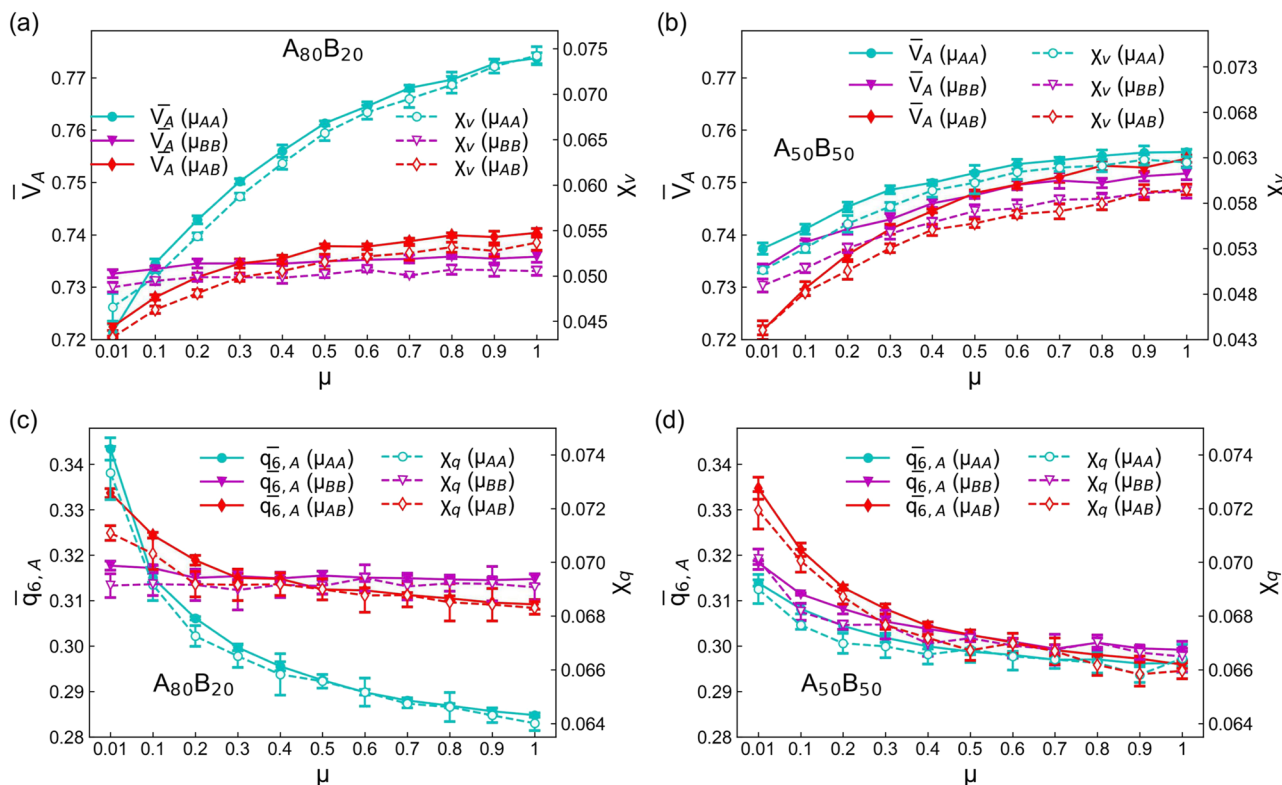


FIG. 3. Changes in the mean and standard deviation of the Voronoi volume and bond-orientational order parameter. (a) and (b) The mean value (\bar{V}_A) and standard deviation (X_V) of the Voronoi volume of A particles. (c) and (d) The mean value ($\bar{q}_{6,A}$) and standard deviation (X_q) of the bond-orientational order parameter of A particles.

full icosahedron, which is denoted by the Voronoi index $\langle 0, 0, 12, 0 \rangle$, is found to be less than 0.6%, as shown in Figs. 4(a) and 4(b). However, this lack of icosahedra does not undermine the importance of fivefold local symmetry, which is the most abundant one among the various local symmetries, as shown in Figs. 4(c) and 4(d). As we will see later, the prevalence of fivefold local ordering will give rise to the orientational order present on the intermediate-range scale.

Apart from these nearest neighbor-based structural quantities, the radial distribution function $g(r)$ is often used to characterize the structure of disordered systems. Figures 5(a) and 5(b) show $g(r)$ for several different combinations of friction coefficients for the two compositions. One sees that the dependence of $g(r)$ on friction is rather weak, with the impact of μ_{AA} only discernible for $A_{80}B_{20}$, due to the dominant role of μ_{AA} relative to the other two friction coefficients in the $A_{80}B_{20}$ system (see also Fig. 3). Compared with μ_{AA} , the effects of μ_{AB} and μ_{BB} are basically undetectable from $g(r)$. Closely related to $g(r)$, the static structure factor $S(q)$ in Figs. 5(c) and 5(d)

is also not sensitive to the change of friction. These results indicate that conventional two-point correlation methods may have difficulty in reflecting the impact of friction on the structure of hard-sphere systems.

In order to understand the influence of friction on the structure on larger length scales, it is instructive to use higher order structural quantities.¹³ In particular, we used the four-point correlation function as mentioned earlier to probe the 3D structure of the systems. The first step of using this method is to construct a local coordinate system by selecting a triplet of A particles that are the nearest neighbors to each other. Then, one defines the position of particle 1 as the origin, and the direction from particle 1 to particle 2 as the z axis. The plane in which the three particles are located is defined as the x - z plane, with the y axis being perpendicular to that plane. With this local coordinate system, we can determine the 3D distribution of particles at a distance r from the origin, i.e., a four-point correlation. In the structural analysis, we excluded particles within

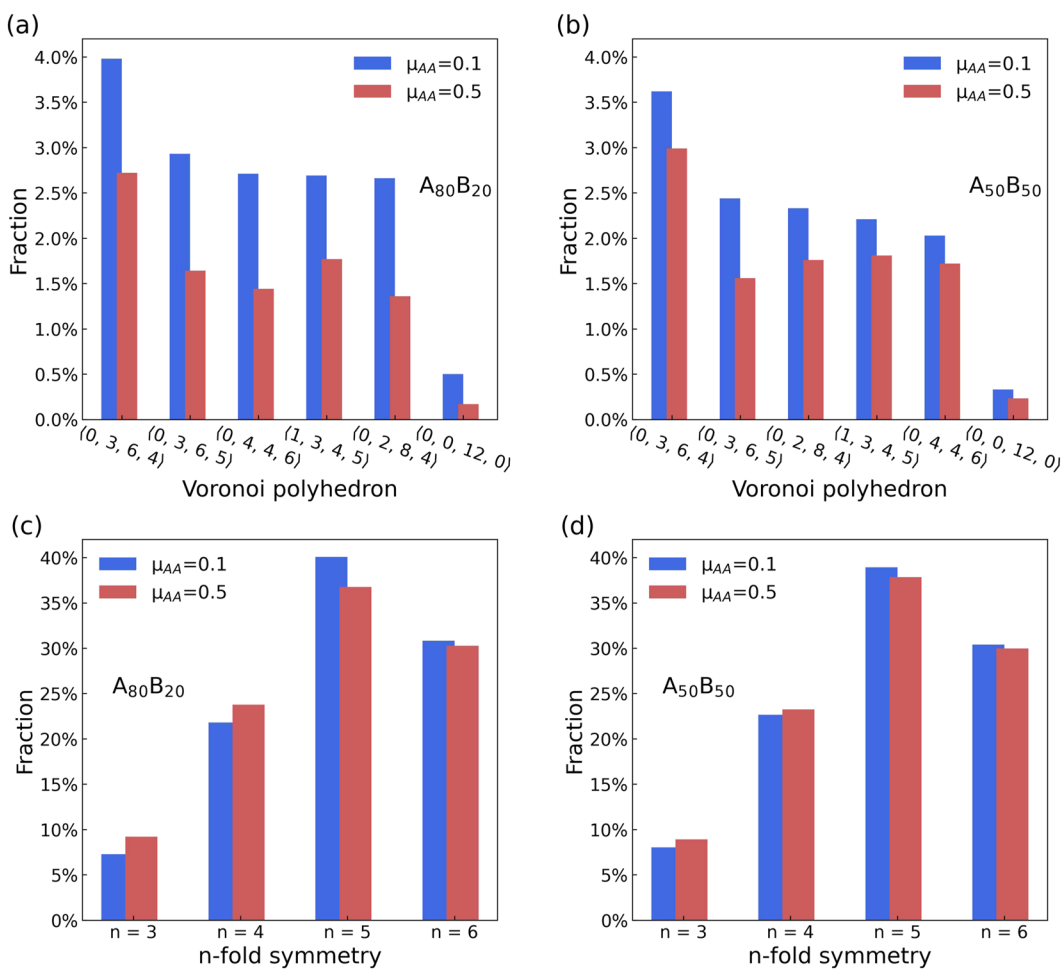


FIG. 4. (a) and (b) Percentage of the five most frequent polyhedra types (from left to right) and the full icosahedron $\langle 0, 0, 12, 0 \rangle$ for the $A_{80}B_{20}$ and $A_{50}B_{50}$ systems, respectively. (c) and (d) Percentage of threefold, fourfold, fivefold, and sixfold symmetries for the $A_{80}B_{20}$ and $A_{50}B_{50}$ systems, respectively. The compression rate is $0.004 \tau^{-1}$ with $\mu_{BB} = 0.2$ and $\mu_{AB} = 0.3$.

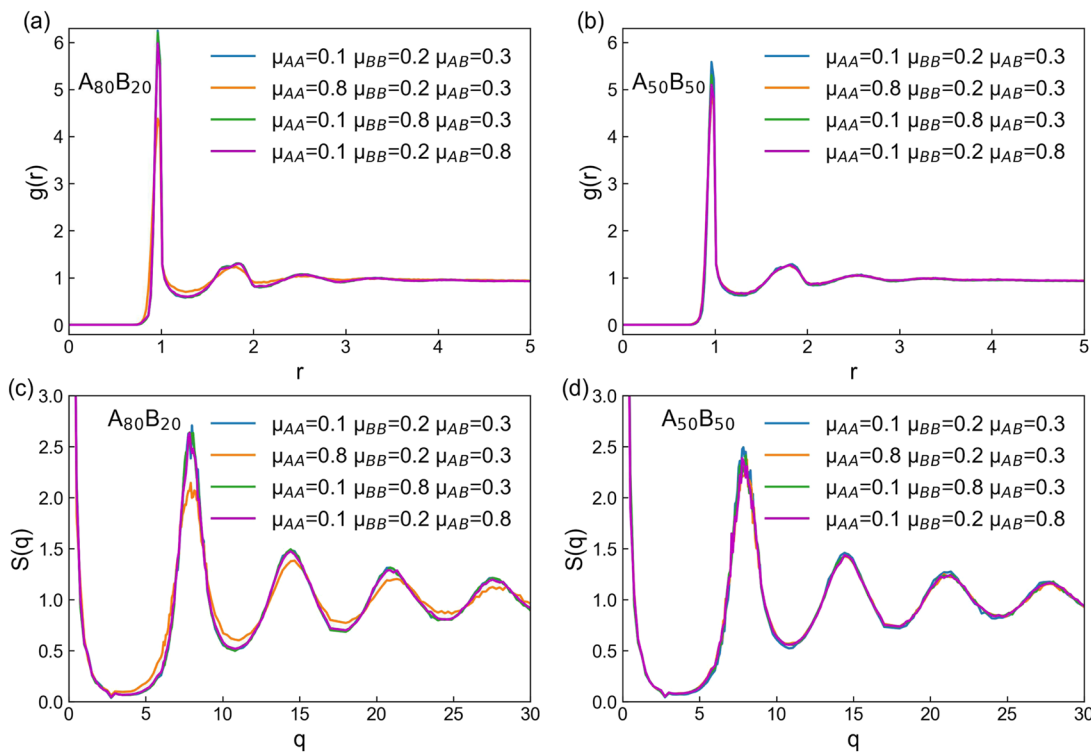


FIG. 5. Radial distribution function $g(r)$ and static structure factor $S(q)$. (a) and (b) $g(r)$ for different combinations of friction coefficients for $A_{80}B_{20}$ and $A_{50}B_{50}$, respectively. (c) and (d) $S(q)$ for different combinations of concentration and friction. $S(q)$ jumps to a large value as $q \rightarrow 0$, a result that may be related to the fact that the analyzed sample (after removing the particle layers close to the wall) is only finite.

09 June 2024 06:55:43

4 d from the box wall to avoid potential artificial (crystallized) packing structures.

Figure 6(a) illustrates the density distribution $\rho(r, \theta, \phi)$ of type A particles within a spherical shell of thickness $0.4d$. As the central particle is also of type A, this is referred to as AA-correlation. It is evident that the density distribution is r -dependent and highly symmetric at some selected distances. One observes that an icosahedral and dodecahedral symmetry alternate with increasing r . This result can be rationalized by considering that the positions of the low-density regions (cavities) in the density distribution at a given r become high density spots in the subsequent layer of the packing structure, i.e., these two symmetries are dual to each other.

Similar evolution of structural symmetries is also present in other systems, as shown in Figs. 6(b)–6(e). However, unlike the $g(r)$ and $S(q)$ shown in Fig. 5, the effect of friction on the 3D density distribution is clearly seen: an increase in friction leads to a reduction in the orderliness of the density distribution, e.g., panels (a) and (b), with this difference becoming more pronounced as r increases. It is also interesting to note that in the $A_{80}B_{20}$ system, changing μ_{BB} and μ_{AB} has only a negligible effect on the orientational order among A particles as seen from the 3D density plots. As the concentration of A particles decreases, panel (e) for the $A_{50}B_{50}$ system, the degree of structural order declines relative to the $A_{80}B_{20}$ system, panel (a).

Furthermore, one can quantify the structural order as shown in Fig. 6 by decomposing the density distribution $\rho(r, \theta, \phi)$ using spherical harmonics Y_l^m ,

$$\rho(r, \theta, \phi) = \sum_{l=0}^{\infty} \sum_{m=-l}^l \rho_l^m(r) Y_l^m(\theta, \phi), \quad (6)$$

where θ and ϕ are the two angular variables, and the expansion coefficient ρ_l^m is given by

$$\rho_l^m = \int_0^{2\pi} d\varphi \int_0^\pi d\theta \sin \theta \rho(\theta, \varphi, r) Y_l^{m*}(\theta, \varphi). \quad (7)$$

Then, one takes the square root of the angular power spectrum

$$S_\rho = \left[(2l+1)^{-1} \sum_{m=-l}^l |\rho_l^m(r)|^2 \right]^{\frac{1}{2}} \quad (8)$$

to characterize the anisotropy of the density distribution.

Figures 7(a)–7(c) show the dependence of S_ρ on r in systems with different combinations of friction for $A_{80}B_{20}$. Consistent with previous studies, we find that the mode $l = 6$ has the strongest signal among the various modes and that it best captures the icosahedral symmetry as seen in the 3D density distribution.²⁷ One can see that these curves exhibit oscillatory behavior and decrease exponentially

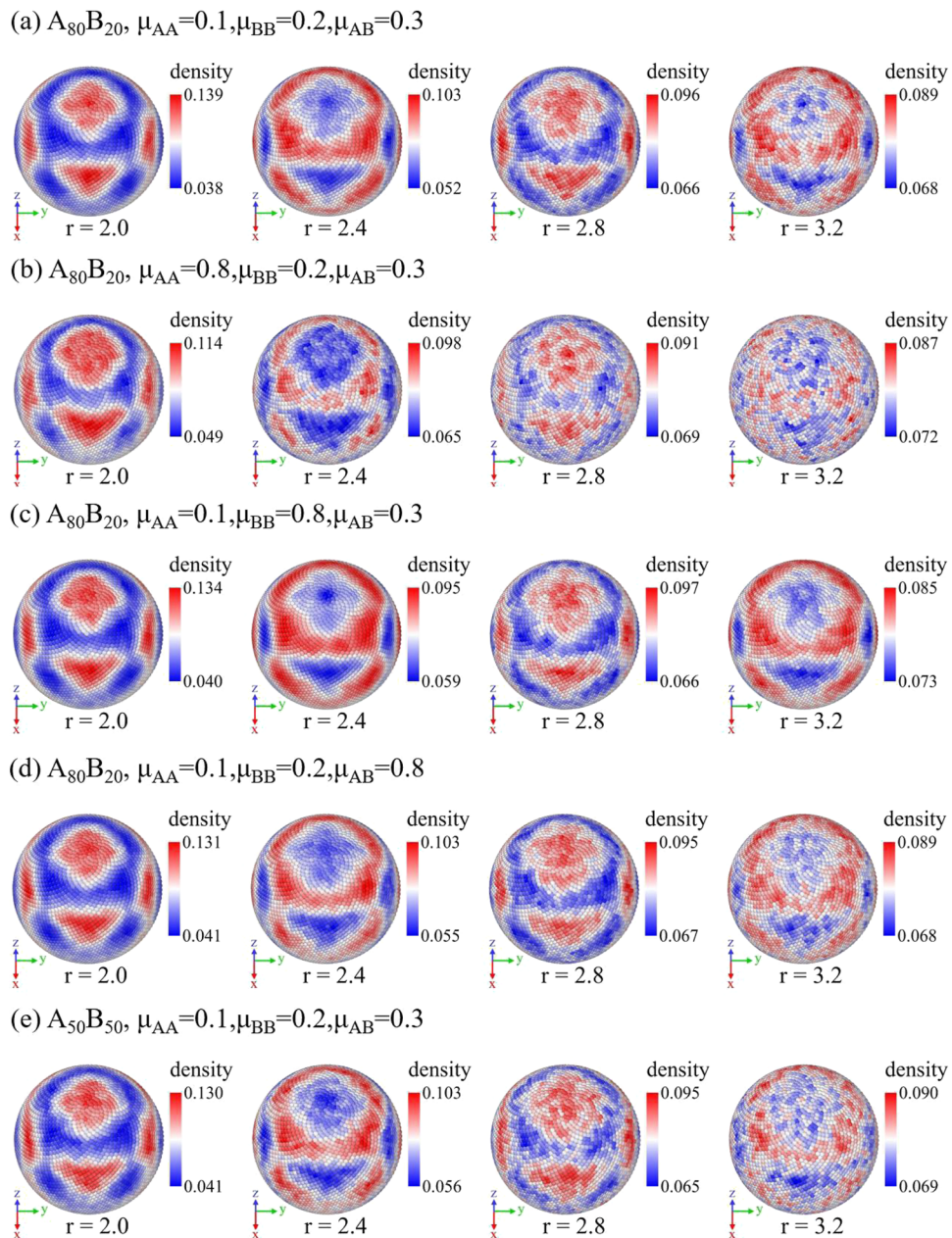


FIG. 6. Three-dimensional density distribution of particles in a spherical shell with a thickness of $0.4d$. Here, we show the AA-correlation.

as r increases. Furthermore, we note that the maxima of these curves correspond to the locations where one finds dodecahedral or icosahedral orientational order, as shown in Fig. 6. Interestingly, one observes that the distances at which the maxima appear do not seem to be affected by the change of friction. By contrast, the height of these peaks (which indicates the strength of the orientational order) and the slope of the envelope (which characterizes how fast the struc-

tural order decays with increasing r) show notable dependence on friction. Specifically, S_ρ changes significantly when μ_{AA} is increased from 0.01 to 0.5 but then saturates with further increase of μ_{AA} , panel (a). In contrast, one recognizes from panel (b) that the change of μ_{BB} barely affects S_ρ . μ_{AB} has a moderate influence on S_ρ . More quantitatively, we have measured the decay length ξ of the 3D structure by fitting the maxima of S_ρ using the expression $y = A \exp(-r/\xi)$,

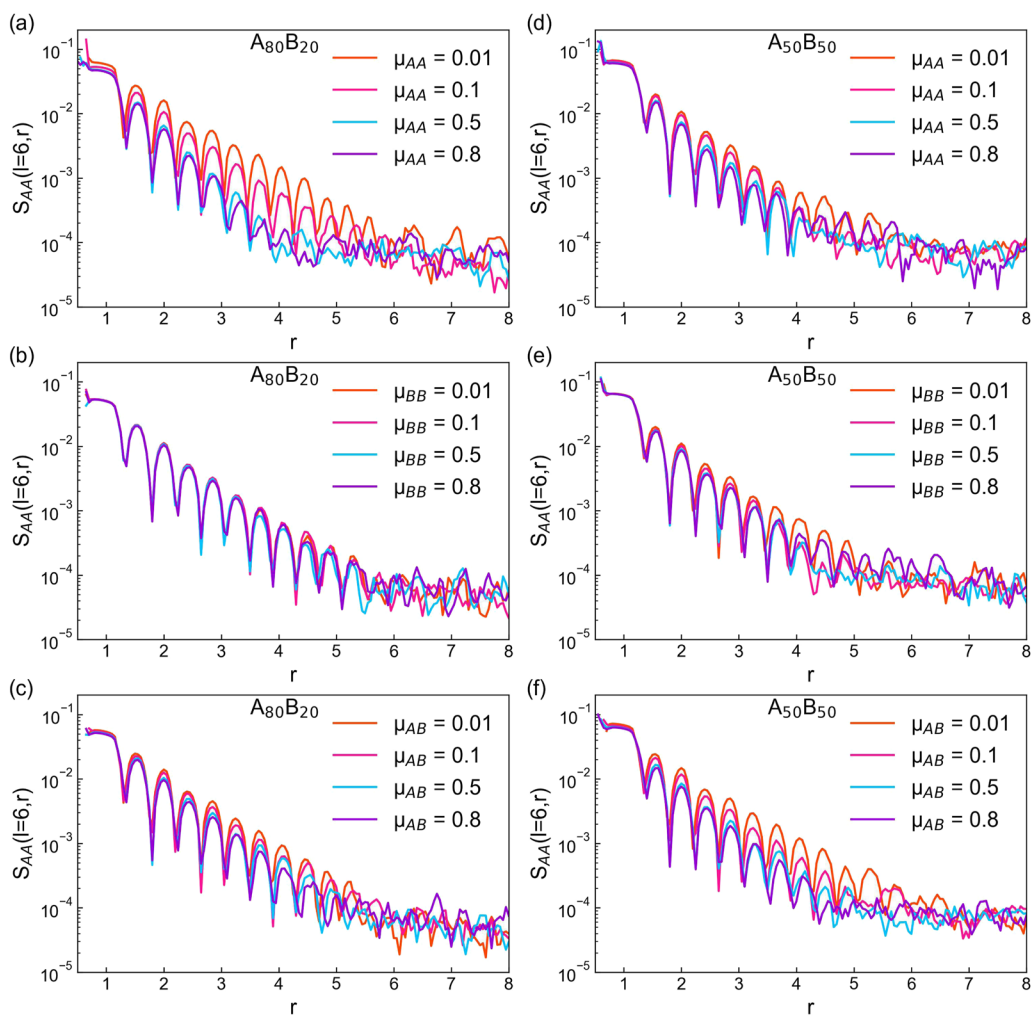


FIG. 7. $S_p(l = 6, r)$ of AA-correlation in systems with different combinations of friction coefficients. (a)–(c) $A_{80}B_{20}$. (d)–(f) $A_{50}B_{50}$.

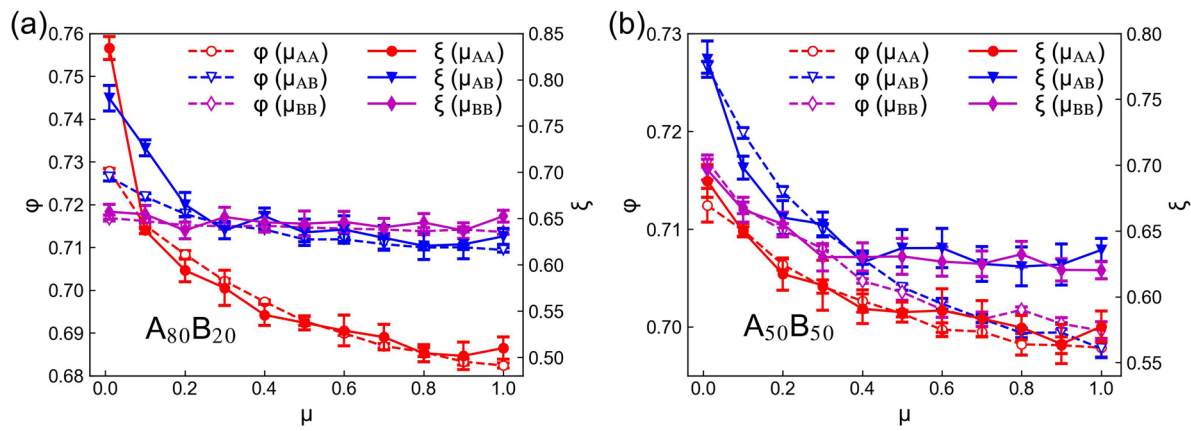


FIG. 8. The dependence of packing fraction φ and length scale ξ on different friction coefficients. (a) $A_{80}B_{20}$. (b) $A_{50}B_{50}$.

where A is a fitting parameter, and the results are presented in Fig. 8(a) for $\text{A}_{80}\text{B}_{20}$.

For $\text{A}_{50}\text{B}_{50}$ [Figs. 7(d)–7(f)], one recognizes that the strongest effect of friction on S_p comes from μ_{AB} , while the influence of μ_{AA} and μ_{BB} is relatively weak; this is also reflected in the change of decay length with friction, as shown in Fig. 8(b).

Also presented in Fig. 8 is the packing fraction φ , defined as $\varphi = \sum_i v_i / \sum_i v_{\text{voro},i}$, where v_i and $v_{\text{voro},i}$ are, respectively, the volume and Voronoi volume of particle i . For both compositions, φ decreases with increasing friction, in accordance with the decrease of ξ . This result indicates that the local packing of particles becomes less efficient along with a faster decay of the structural order. We note that the consistency between the change of packing friction and decay length contrasts with the variation trend between the two previously observed in binary hard-sphere mixtures with zero friction.²⁸ Hence, one can conclude that friction plays an important role not only in determining the local packing structure but also in how these structures grow and evolve on larger length scales.

IV. CONCLUSIONS

Our simulations have demonstrated that friction is an important factor controlling the structure of hard-sphere mixtures. Using Voronoi volume and bond-orientational order parameters to characterize the local structure, we found that the three friction coefficients have a similar effect on the local structure of the system, i.e., the structure becomes more disordered with increasing friction, while the influence from a given type of particle increases as one increases its concentration. We also demonstrated that the standard two-point correlation functions, i.e., the radial distribution function and static structure factor, can barely show differences brought by changing friction in the structure beyond the nearest neighbor coordination shell. In contrast, a recently introduced four-point structural method revealed the presence of an alternating dodecahedral–icosahedral orientational order on the intermediate and large length scales; the origin of this intermediate-range order can be attributed to the presence of pronounced fivefold local symmetry in the structure. It is also found that the strength of this order and the structural decay length depend on inter-particle friction, particularly the ones associated with the more abundant particle species. Finally, we found that in contrast to the case where there is no friction between the particles, the local packing efficiency and the decay length are positively correlated when inter-particle frictions come into effect. This difference might also be related to the different size ratios between the two types of particles and the fact that friction affects not only the local packing structure but also how these local structural motifs are organized to form a structure on the intermediate and large length scales.

SUPPLEMENTARY MATERIAL

We document in the supplementary material the influence of the simulation protocol on the short-to-intermediate range structure and some additional analyses on bond-orientational order parameters to further support our simulations.

ACKNOWLEDGMENTS

We acknowledge Walter Kob for fruitful discussion and comments. This study was supported by the National Natural Science Foundation of China (Grant Nos. 12274292, 11504033) and the China Scholarship Council (No. 202208510112).

AUTHOR DECLARATIONS

Conflict of Interest

The authors have no conflicts to disclose.

Author Contributions

Jiajun Tang: Data curation (equal); Formal analysis (equal); Methodology (equal); Software (equal); Writing – original draft (equal). **Xiaohui Wen:** Conceptualization (equal); Funding acquisition (equal); Methodology (equal); Project administration (equal); Resources (equal); Supervision (equal); Writing – review & editing (equal). **Zhen Zhang:** Conceptualization (equal); Investigation (equal); Methodology (lead); Supervision (equal); Writing – review & editing (lead). **Devin Wang:** Methodology (equal); Supervision (equal); Validation (equal). **Xinbiao Huang:** Data curation (equal); Investigation (equal). **Yujie Wang:** Conceptualization (equal); Funding acquisition (equal); Methodology (equal); Supervision (equal); Writing – review & editing (equal).

DATA AVAILABILITY

The data that support the findings of this study are available from the corresponding authors upon reasonable request.

REFERENCES

- ¹H. A. Makse, D. L. Johnson, and L. M. Schwartz, *Phys. Rev. Lett.* **84**, 4160 (2000).
- ²G. Y. Onoda and E. G. Liniger, *Phys. Rev. Lett.* **64**, 2727 (1990).
- ³J. G. Berryman, *Phys. Rev. A* **27**, 1053 (1983).
- ⁴M. D. Rintoul and S. Torquato, *Phys. Rev. Lett.* **77**, 4198 (1996).
- ⁵J. Finney, *Proc. R. Soc. London, Ser. A* **319**, 479 (1970).
- ⁶G. D. Scott, *Nature* **188**, 908 (1960).
- ⁷J. Bernal and J. Mason, *Nature* **188**, 910 (1960).
- ⁸K. Binder and W. Kob, *Glassy Materials and Disordered Solids: An Introduction to Their Statistical Mechanics* (World Scientific, Singapore, 2011).
- ⁹P. S. Salmon, *J. Phys.: Condens. Matter* **18**, 11443 (2006).
- ¹⁰J.-P. Hansen and I. R. McDonald, *Theory of Simple Liquids* (Elsevier, Amsterdam, 1990).
- ¹¹N. W. Ashcroft and N. D. Mermin, *Solid State Physics* (Holt Rinehart and Winston, New York, 1976).
- ¹²H. Tong and H. Tanaka, *Phys. Rev. X* **8**, 011041 (2018).
- ¹³C. P. Royall and S. R. Williams, *Phys. Rep.* **560**, 1 (2015).
- ¹⁴V. Ogarko and S. Luding, *Soft Matter* **9**, 9530 (2013).
- ¹⁵Y. Q. Cheng and E. Ma, *Prog. Mater. Sci.* **56**, 379 (2011).
- ¹⁶R. S. Farr and R. D. Groot, *J. Chem. Phys.* **131**, 244104 (2009).
- ¹⁷M. Clusel *et al.*, *Nature* **460**, 611 (2009).
- ¹⁸D. Coslovich and G. Pastore, *J. Chem. Phys.* **127**, 124504 (2007).
- ¹⁹M. Leocmach and H. Tanaka, *Nat. Commun.* **3**, 974 (2012).
- ²⁰S. Torquato and F. H. Stillinger, *Rev. Mod. Phys.* **82**, 2633 (2010).

- ²¹G. Parisi and F. Zamponi, *Rev. Mod. Phys.* **82**, 789 (2010).
- ²²K. Watanabe and H. Tanaka, *Phys. Rev. Lett.* **100**, 158002 (2008).
- ²³C. Song, P. Wang, and H. A. Makse, *Nature* **453**, 629 (2008).
- ²⁴S. Torquato and H. Haslach, *Appl. Mech. Rev.* **55**, B62 (2002).
- ²⁵T. Kawasaki, T. Araki, and H. Tanaka, *Phys. Rev. Lett.* **99**, 215701 (2007).
- ²⁶H. Shintani and H. Tanaka, *Nat. Phys.* **2**, 200 (2006).
- ²⁷Z. Zhang and W. Kob, *Proc. Natl. Acad. Sci. U. S. A.* **117**, 14032 (2020).
- ²⁸H. F. Yuan *et al.*, *Phys. Rev. Lett.* **127**, 278001 (2021).
- ²⁹N. Singh *et al.*, *Proc. Natl. Acad. Sci. U. S. A.* **120**, e23009 (2023).
- ³⁰A. Lemaitre *et al.*, *Phys. Rev. Lett.* **126**, 075501 (2021).
- ³¹A. Lemaitre *et al.*, *Phys. Rev. B* **103**, 054110 (2021).
- ³²A. P. Santos *et al.*, *Phys. Rev. E* **102**, 032903 (2020).
- ³³L. E. Silbert, *Soft Matter* **6**, 2918 (2010).
- ³⁴N. Vandewalle *et al.*, *Eur. Phys. J. E* **22**, 241 (2007).
- ³⁵L. E. Silbert, G. S. Grest, and J. W. Landry, *Phys. Rev. E* **66**, 061303 (2002).
- ³⁶Y. Yuan *et al.*, *Phys. Rev. Lett.* **127**, 018002 (2021).
- ³⁷X. L. Sun *et al.*, *Phys. Rev. Lett.* **125**, 268005 (2020).
- ³⁸S. Papanikolaou, C. S. O'Hern, and M. D. Shattuck, *Phys. Rev. Lett.* **110**, 198002 (2013).
- ³⁹M. Jerkins *et al.*, *Phys. Rev. Lett.* **101**, 018301 (2008).
- ⁴⁰S. Plimpton, *J. Comput. Phys.* **117**, 1 (1995).
- ⁴¹L. Vu-Quoc and X. Zhang, *Mech. Mater.* **31**, 235 (1999).
- ⁴²G. K. P. Barrios *et al.*, *Powder Technol.* **248**, 84 (2013).
- ⁴³A. Di Renzo and F. P. Di Maio, *Chem. Eng. Sci.* **60**, 1303 (2005).
- ⁴⁴H. A. Makse *et al.*, *Phys. Rev. E* **70**, 061302 (2004).
- ⁴⁵P. J. Steinhardt, D. R. Nelson, and M. Ronchetti, *Phys. Rev. B* **28**, 784 (1983).
- ⁴⁶N. P. Walter *et al.*, *Comput. Phys. Commun.* **228**, 209 (2018).
- ⁴⁷Y. C. Hu and H. Tanaka, *Sci. Adv.* **6**, eabd2928 (2020).
- ⁴⁸V. A. Levashov, R. Ryltsev, and N. Chtchelkatchev, *Soft Matter* **15**, 8840 (2019).